Electronic Supplementary Information

Solution-processed chalcopyrite-perovskite tandem solar cells in bandgap-matched two- and four-terminal architectures

Alexander R. Uhl,[‡*a] Zhibin Yang,[‡b] Alex K.-Y. Jen,*[bc] Hugh W. Hillhouse*[a]

[a] Department of Chemical Engineering, University of Washington, Seattle, WA 98195, USA

[b] Department of Materials Science and Engineering, University of Washington, Seattle, WA 98195, USA

[c] Department of Biology and Chemistry, City University of Hong Kong, Kowloon, HK

* E-mail: auhl@uw.edu, ajen@uw.edu, h2@uw.edu

[‡] These authors contributed equally to this work.

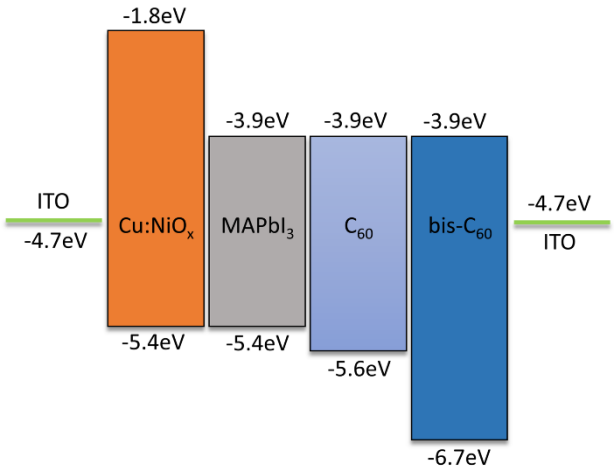

Figure S1: Energy level diagram of our semi-transparent $MAPbI_3$ perovskite solar cell as predicted from reported literature values.[1-3] Single values represent work functions while values on bands represent conduction and valence band levels.

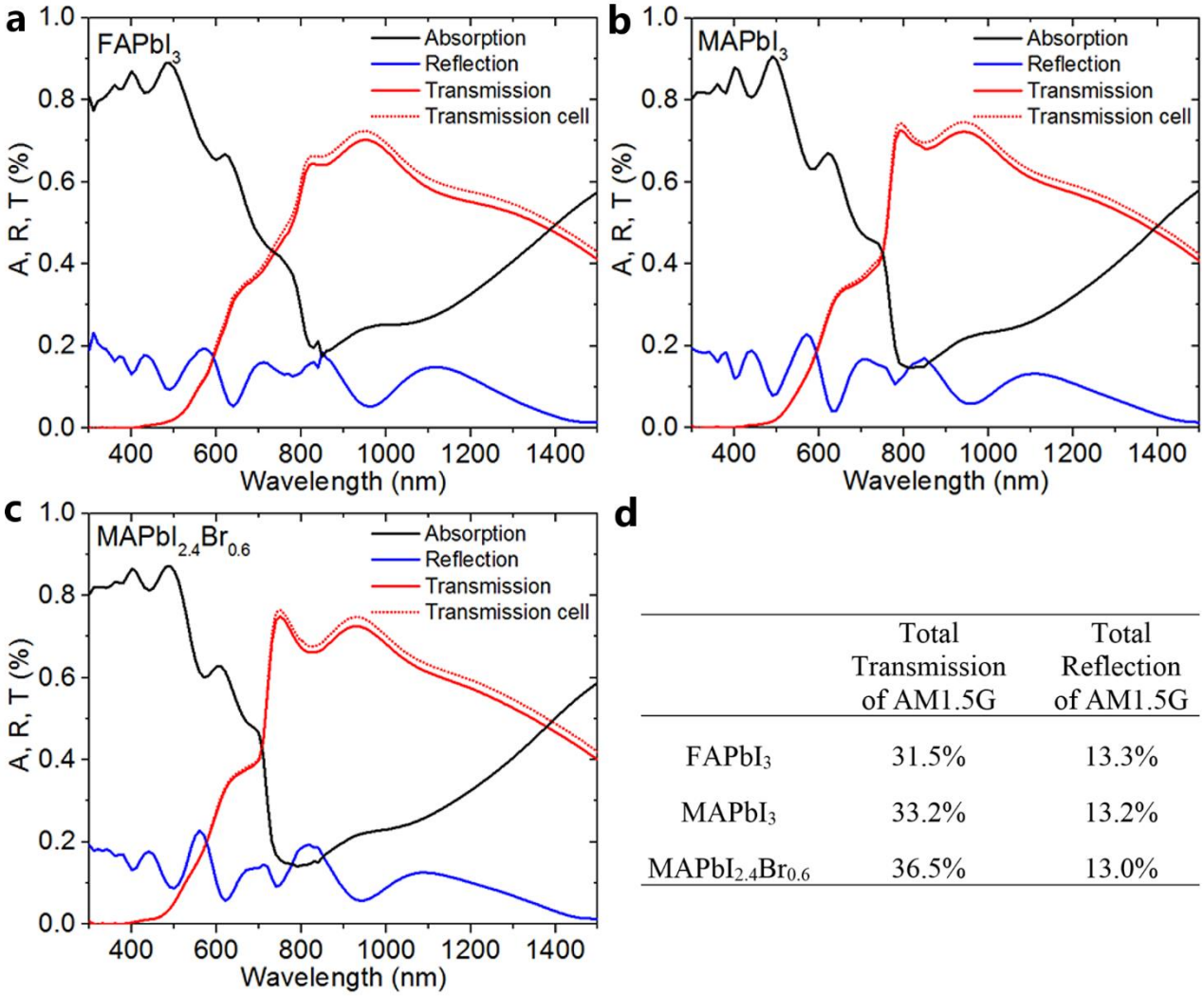

	Total Transmission of AM1.5G	Total Reflection of AM1.5G
$FAPbI_3$	31.5%	13.3%
$MAPbI_3$	33.2%	13.2%
$MAPbI_{2.4}Br_{0.6}$	36.5%	13.0%

Figure S2: (a-c) Optical spectra of the perovskite cells (dashed line) from Table 1 and the respective filters (solid line) that were used to determine the performance of the shaded chalcogenide cells. (d) Calculated total transmission and reflection values for the respective perovskite filters based on the total photon flux of the AM1.5G spectrum.

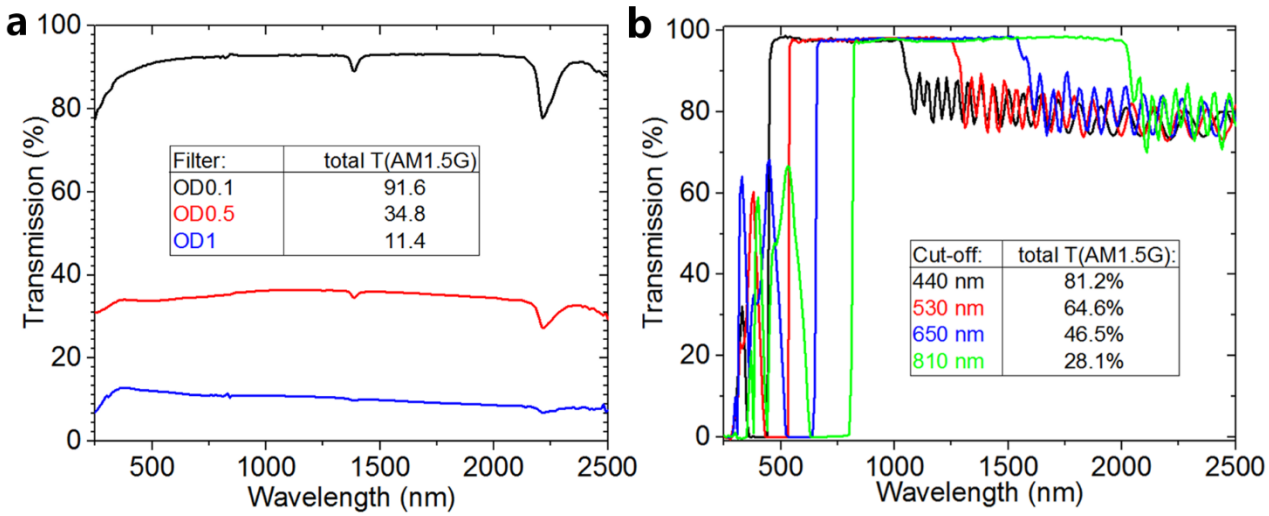

Figure S3: (a) Transmission spectra for the employed neutral density filters, i.e. OD 0.1, OD 0.5, and OD 1 and (b) long-pass (LP) filters at various cut-off wavelengths, i.e. 440 nm, 530 nm, 650 nm, and 810 nm. LP filters of higher wavelengths were used in addition with shorter-wavelength filters to omit UV bleeding during the measurement. The total transmission of the AM1.5G photon flux is calculated for the OD filters and effective LP filter combinations.

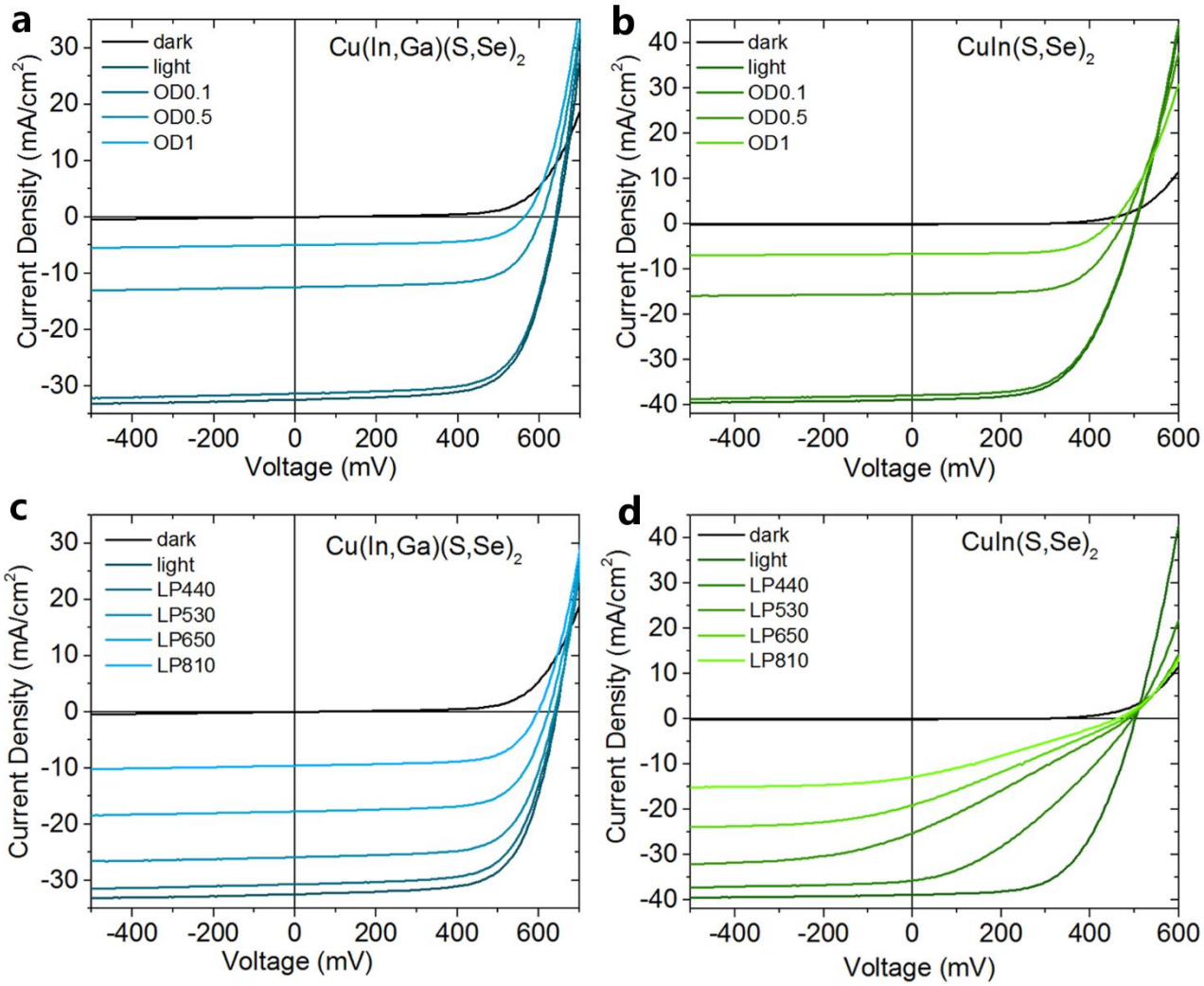

Figure S4: Low-light performance of CIGS (a, c) and CIS devices (b, d). Neutral density filters with various optical density (OD) of 0.1, 0.5, and 1 (a, b) and long pass (LP) filters of 440 nm, 530 nm, 650 nm, and 810 nm (c, d) were employed for this experiment (See Fig. S2). The lack of the UV portion of the light leads to a pronounced FF loss in case of the Ga-free samples. Photo-doping of the CdS buffer layer combined with a larger CBO for CIS as compared to CIGS samples is held accountable for that phenomenon. All performance relevant values are summarized in Table S1.

Table S1: Performance data of filtered CIGS and CIS devices (Fig. 2 a - d). The transmission values of the used filters and respective cell PCE was estimated from the measured short circuit current of a Si diode.

	Condition	T (%)	Rs (Ohm cm^2)	Rsh (Ohm cm^2)	Voc (mV)	Jsc (mA/cm^2)	FF (%)	PCE with filter (%)	PCE (%)
CIGS	baseline	100	2.24	554	643	32.5	68.2	14.2	14.2
	OD 0.1	97	2.18	715	638	31.4	68.6	13.7	14.2
	OD 0.5	38	4.08	844	603	12.5	68.3	5.14	13.6
	OD 1	14	8.32	1020	560	5.01	65.1	1.83	13.0
	LP 440 nm	93	2.50	637	642	30.7	67.6	13.3	14.3
	LP 530 nm	76	2.96	609	638	25.9	68.1	11.2	14.8
	LP 650 nm	54	3.63	721	623	17.7	68.6	7.59	14.1
	LP 810 nm	30	5.32	823	597	9.58	67.9	3.88	13.0
CIS "low S"	baseline	100	2.94	537	502	38.9	58.5	11.4	11.4
	OD 0.1	97	2.89	474	500	37.9	59.1	11.2	11.6
	OD 0.5	38	5.06	1070	473	15.5	63.3	4.65	12.3
	OD 1	14	9.34	1960	444	6.68	64.5	1.91	13.6
	LP 440 nm	93	6.71	83	495	35.6	35.6	6.26	6.73
	LP 530 nm	76	12.9	29	485	25.2	26.9	3.28	4.33
	LP 650 nm	54	16.5	38	474	19.0	27.9	2.51	4.65
	LP 810 nm	30	21.0	69	460	12.8	28.9	1.70	5.69

Table S2: Performance data of the champion CIS device used in Fig. 2 e, f and Table 1. The transmission values of the used filters and respective cell PCE after the filters was estimated from the measured short circuit current of a calibrated Si diode.

	Condition	T (%)	Rs (Ohm cm^2)	Rsh (Ohm cm^2)	Voc (mV)	Jsc (mA/cm^2)	FF (%)	PCE with filter (%)	PCE (%)
CIS "high S"	baseline	100	2.07	565	506	39.2	65.7	13.0	13.0
	OD 0.1	97	2.15	627	501	37.4	65.9	12.3	12.7
	OD 0.5	38	3.86	901	473	16.0	66.9	5.06	13.4
	OD 1	14	6.55	1131	438	6.32	66.4	1.84	13.1
	LP 440 nm	93	2.47	560	501	37.3	63.6	11.9	12.8
	LP 530 nm	76	2.91	634	500	31.6	63.2	9.96	13.1
	LP 650 nm	54	3.42	799	490	23.6	64.4	7.46	13.8
	LP 810 nm	30	4.32	976	473	15.0	65.9	4.69	15.7

Table S3: Inductively coupled plasma mass spectroscopy (ICP-MS) compositional study (in at.%) for the $CuIn(S,Se)_2$ absorbers that were used in Fig. 2 c, d and Fig. 2 e, f, respectively. Stable FF and increasing performance at UV-filtered light was seen for the cell with higher S/Se ratio.

	Cu/In	S/Se
$CuIn(S,Se)_2$ "low S"	0.95 ± 0.02	0.009 ± 0.002
$CuIn(S,Se)_2$ "high S"	1.03 ± 0.02	0.058 ± 0.002

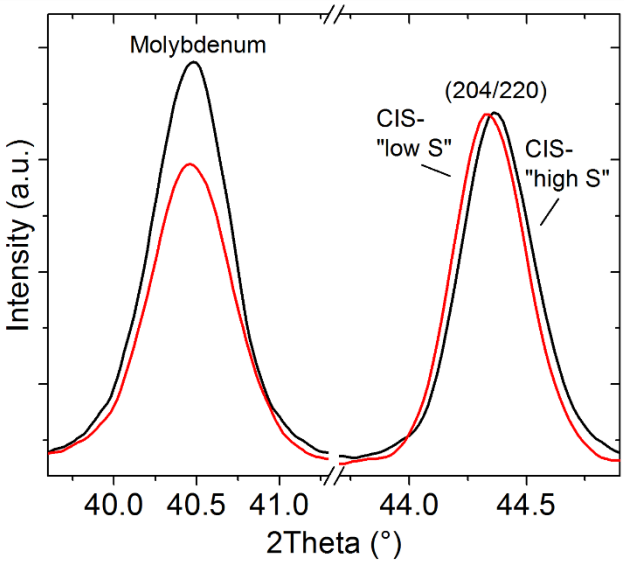

Figure S5: X-ray diffraction measurement of $CuIn(S,Se)_2$ absorbers from Fig. 2 c, d and Fig. 2 e, f. The peak shift to higher diffraction angles for the latter can be explained by higher S/Se ratio, corroborating findings with ICP-MS (Table S3). The Molybdenum substrate peak is shown as reference to confirm the accurate substrate alignment during the measurement.

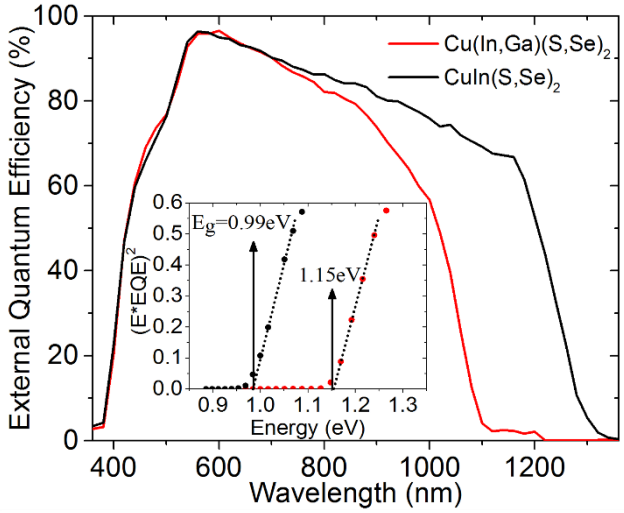

Figure S6: External Quantum Efficiency (EQE) spectra of the chalcogenide cells from Table 1 and their respective bandgaps.

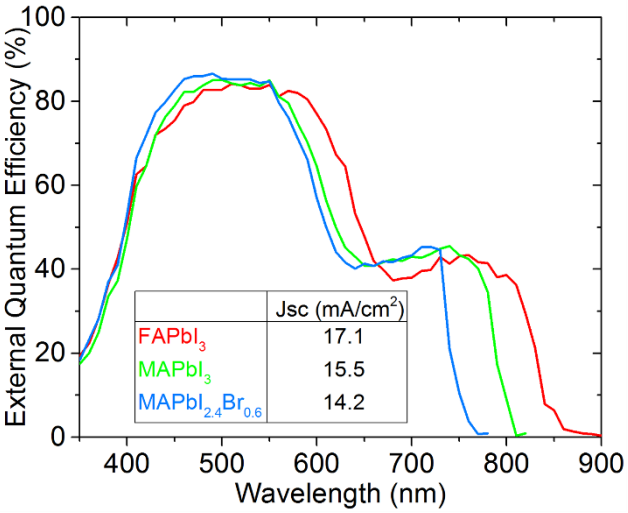

Figure S7: EQE spectra of the perovskite cells from Table 1 and their respective current densities as calculated from EQE.

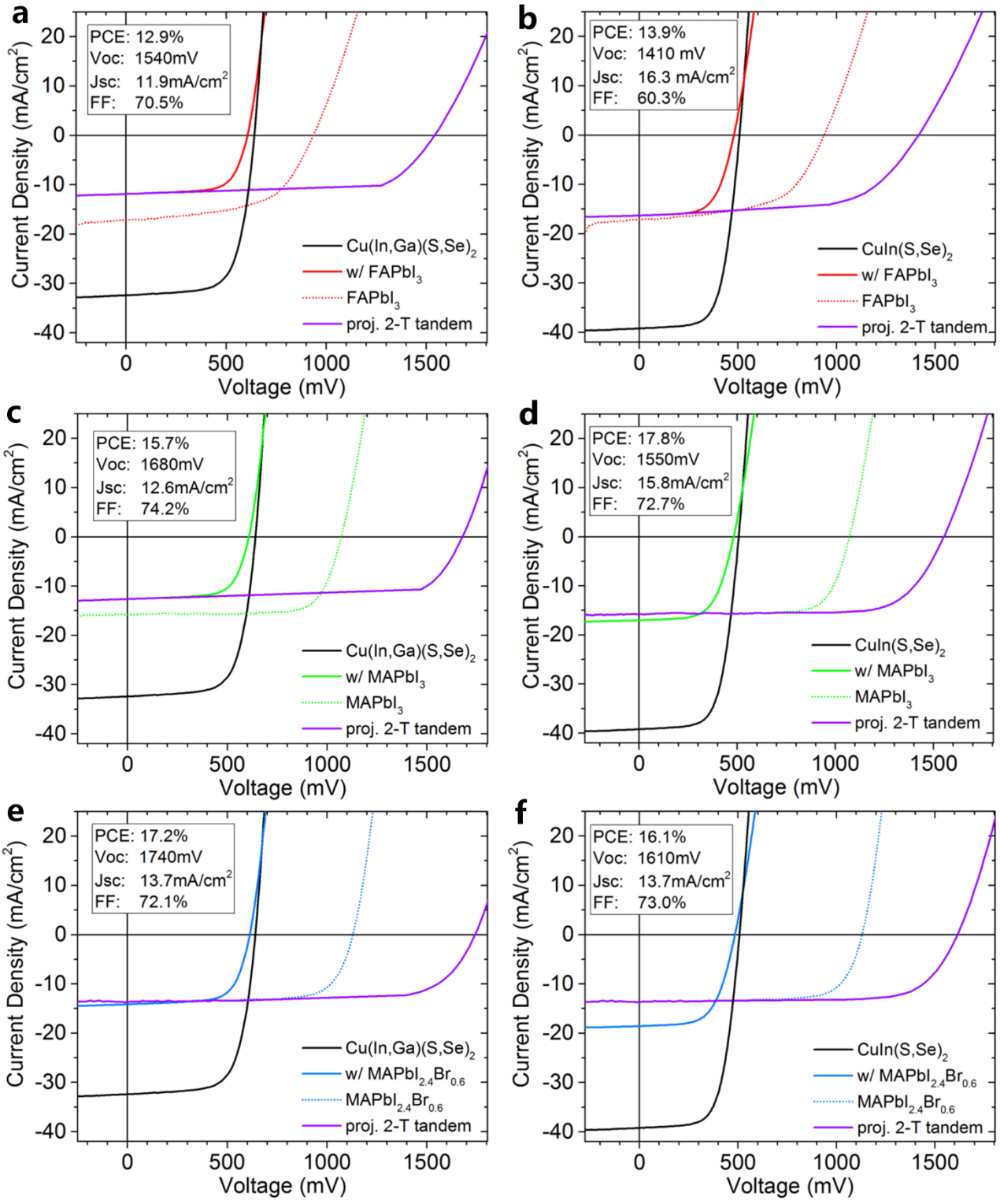

Figure S8: Projected two-terminal tandem efficiencies from J(V) data of $FAPbI_3$ (a, b), $MAPbI_3$ (c, d), and $MAPbI_{2.4}Br_{0.6}$ top cells (e, f) with $Cu(In,Ga)(S,Se)_2$ (left column) and $CuIn(S,Se)_2$ bottom cells (right column). Projected efficiencies with stabilized perovskites are shown in Fig. S9.

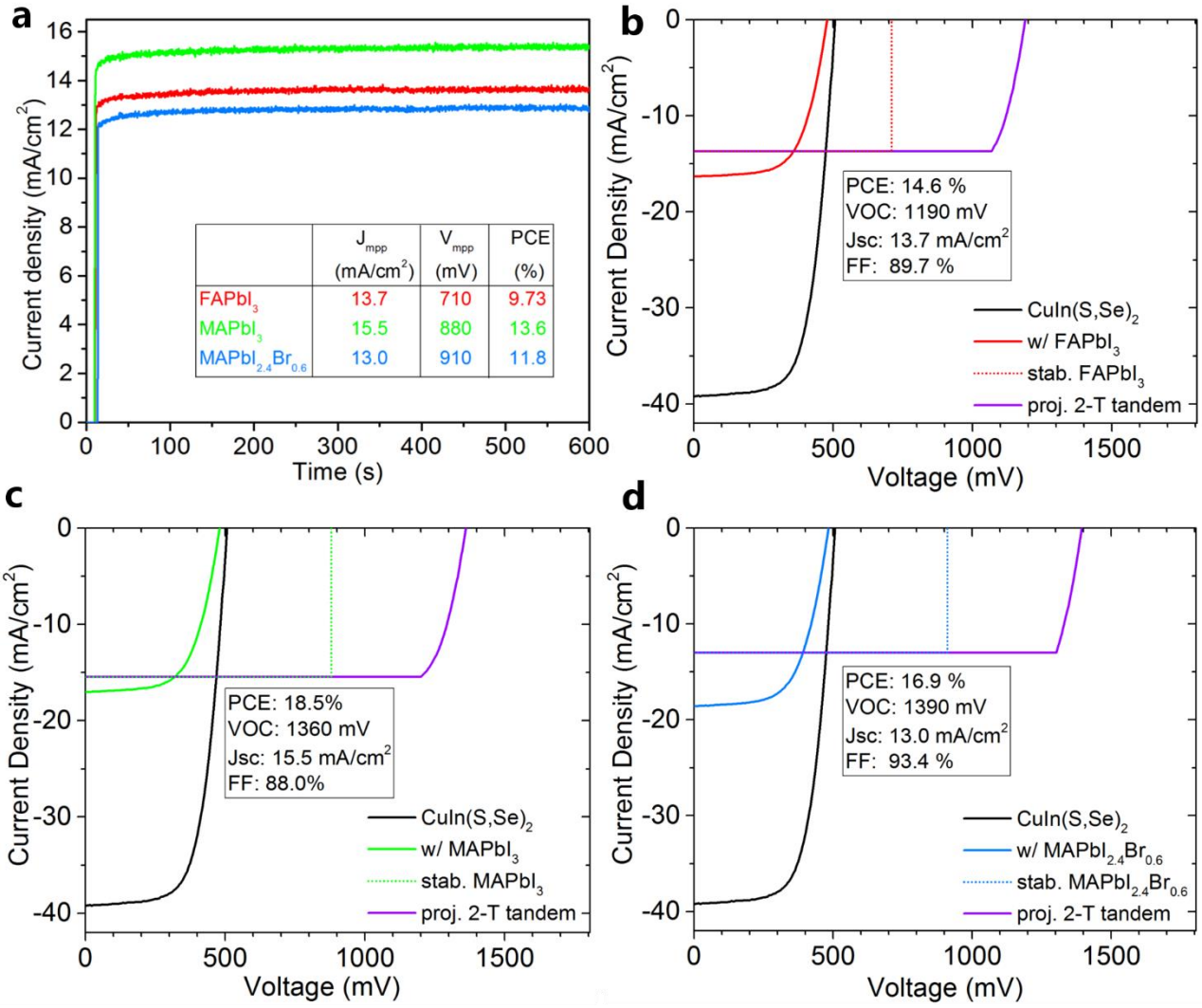

Figure S9: (a) Measurement of the stabilized power output of the perovskite cells that were used in this work. The steady-state photocurrent of the $FAPbI_3$, $MAPbI_3$, and $MAPbI_{2.4}Br_{0.6}$ cells was determined after 600 s of constant illumination at the maximum power point with applied voltages of 0.71 V, 0.88 V, and 0.91 V, respectively. (b-d) Projected two-terminal tandem efficiencies with stabilized perovskite cells and CIS bottom cells. Highest two-terminal efficiencies of 18.5% are projected for tandem devices with $CuIn(S,Se)_2$ and $MAPbI_3$ cells.

Preparation of perovskite and chalcopyrite devices

Bifacial hybrid perovskite cells and filters

Materials: Lead iodide, lead bromide and all the solvent used in this work were purchased from Sigma-Aldrich. C_{60} was purchased from American Dye Source, Inc. MAI and FAI was synthesized according to the reported method.[4] Bis-C_{60} was synthesized as reported in our previous work.[5]

Solution preparation: Different perovskite precursors (1 M) were prepared by dissolving PbI_2, $PbBr_2$, MAI and FAI with different ratio into a dimethyl sulphoxide and γ-butyrolactone mixed solvent (volume ratio of 3:7) and stirred at 60°C for 1 hour. 15 mg/ml C_{60} solution were prepared in dichlorobenzene. 2 mg/ml bis-C_{60} surfactant solution was prepared in isopropyl alcohol, followed by sonication for an hour. The NiO_x precursor was prepared according our previous work.[6]

Cell fabrication: ITO glass (15 Ω sq^{-1}) was cleaned by detergent and ultrasonicated in deionized water, acetone, and isopropanol alcohol for 10 minutes, respectively. The ITO glass was further treated by an UV ozone cleaner for 10 minutes after drying with a nitrogen flow. Then, the NiO_x precursor was spin-coated onto the ITO substrate at 3000 rpm for 60 s and annealed at 400°C for 1 hour in air to form the hole transporting layer. Perovskite precursors (filtered with a 0.22 µm PTFE filter) were then spin-coated onto the substrate at 1000 rpm for 15 s and 4000 rpm for 45 s sequentially in the glove box. During the last 15 s of the second spin-coating step, the substrate was treated with toluene drop-casting (0.7 mL). The resulting substrates were annealed at 100°C for 10 minutes on a hotplate. Afterward, the C_{60} solution and bis-C_{60} surfactant solution were spin-coated on the perovskite films at 1000 rpm for 60 s and 3000 rpm for 60 s sequentially. The top ITO electrode was sputtered by a softer RF sputtering method with a low power of 150 W and under 3.5 mTorr of Ar (5 nm/min deposition rate). A shadow mask was applied during the ITO deposition which defined the cell area to 10 mm^2. No masks were used for the preparation of the perovskite filters.

Chalcopyrite solar cells

Ink preparation: The ink preparation, deposition, and annealing was carried out in a N_2 filled glove box with controlled O_2 and H_2O content below 20 ppm according to Uhl et al..[7] To prepare the precursor solutions, 2.5 M TU (recrystallized, 99%, Aldrich), 0.38 M CuCl (99.995%, Aldrich), and 0.45 M $InCl_3$ (99.999%, Aldrich) were added to dimethyl sulfoxide solvent (DMSO, 99.9%, Aldrich). The reagents were added consecutively to the ink and allowed to dissolve under stirring before adding the next. After the addition of $InCl_3$, the inks were heated for 2 h at 120°C to form a clear solution. For the gallium containing inks, 0.14 M $GaCl_3$ (99.99%, Aldrich) was additionally added after dissolving 3.0 M thiourea, 0.40 M CuCl, and 0.33 M $InCl_3$ in DMSO.

Solar cell processing: For the precursor samples, inks were filtered with 0.45 µm PTFE filters, spin-coated at 1300 rpm for 1 min on molybdenum-coated soda lime glass substrates, and annealed on a hotplate at 250°C for 2 min. 10 - 13 coating and annealing cycles were used to build the desired layer thickness. The samples were then placed in a graphite box with selenium pellets (99.99%, Aldrich) and annealed at 540°C for 20 min under flowing Ar (99.998%) and pressures close to atmosphere (1000 torr) to convert the precursor films to absorber layers. KCN etching (97%, Fluka) of the absorbers for 1 min in 10 wt.% aqueous solution was carried out for the CIGS and CIS absorbers in Fig. 3. A 30 nm thick CdS layer was deposited on the substrates by chemical bath deposition from an aqueous solution of 1.5 mM $CdSO_4$ (99.996%, Alfa Aesar), 1.9 M NH_4OH (ACS grade, EMS), and 74 mM TU (recrystallized, 99%, Aldrich) for 12 min at 65°C.

The solar cells were finished with a 50 nm i-ZnO and 250 nm ITO layer by RF-sputtering, Ni/Al grid contacts by thermal evaporation (50/1000 nm), and a 110 nm thick MgF_2 layer by e-beam evaporation. The solar cell area was defined by manual scribing to a cell area of 0.11 cm^2.

Characterization of films and devices

Optical Measurements. The transmittance spectra of the perovskite cells were measured by Varian Cary 5000 UV-Vis-NIR. Transmission and absorbance spectra of the employed filters were collected using a PerkinElmer Lambda 1050 UV/Vis/NIR spectrometer equipped with a 150 mm InGaAs integrating sphere in lab atmosphere. The light beam was masked in order to collect local absorbance spectra every 10 nm.

Device Characterization: The J(V) curves and steady-state photocurrent of the perovskite solar cells were measured by a Keithley 2400 Source Meter under illumination by a 450 Watt Oriel xenon lamp with an AM 1.5G filtered solar simulator (1000 W/m^2). The light intensity was precisely calibrated with a standard Si photodiode detector that can be traced back to the standard of the National Renewable Energy Laboratory. The J(V) curves were measured from reverse bias to forward bias with a scan speed of 0.1 V/s. The EQE spectra were measured by combining a monochromated 450 W xenon lamp (Oriel) with a sourcemeter (Keithley 2400) and calculated using a calibrated Si photodiode (OSI-Optoelectronics). Both J(V) and EQE of perovskite cells were measured in superstrate configuration.

The J(V) curves of the chalcopyrite solar cells with and without filters were measured with a source meter (Keithley, 2400) and class AAA solar simulator with AM1.5G spectrum (Newport, Oriel Sol3A). The irradiance of 1000 W/m^2 was confirmed with a calibrated Si photodiode (Newport, 91150V). The current density of this photodiode was also used to estimate the transmission of filters and cell performance of devices with OD and LP filters (Figure 2, Table S1, S2). Alternatively, we estimated the total transmission and irradiance-corrected PCEs from the measured filter transmission data and the spectra of our solar simulator and found agreement within 12% from the values that were estimated with the Si diode. The error of the measured PCEs (Fig. 3, Table 1) and projected PCEs (Table 1) is estimated to be less than 3% and 5%, respectively. The external quantum efficiencies of chalcopyrite devices with and without filters were measured with a source meter (Keithley, 2400) using a chopped monochromatic beam (Oriel, 300 W Xenon lamp) and lock-in amplifier. Calibrated Si (Thorlabs, FDS100-CAL) and Ge photodiodes (Thorlabs, FDG03-CAL) were used as references.

Inductively coupled plasma mass spectroscopy: Elemental concentrations of Cu, In, S, and Se were determined by ICP-MS using a Perkin Elmer DRC-e. Solid samples, i.e. precursor and absorber layers, were scratched off from the substrate with borosilicate pipettes and digested at 80°C for 12 h in 18 MΩ Milli-Q H_2O with 2.0 vol.% H_2O_2 (TraceSELECT grade, Fluka), 0.5 vol.% HCl (99.999%, Aldrich), and 1.5 vol.% HNO_3 (99.999%, Aldrich) solutions. All elements were calibrated from 2 µg/l to 20 mg/l by matrix-matched dilutions from stock solutions (1000 mg/l, Fluka Analytical). The measurements were carried out in the dynamic reaction cell mode (DRC) with NH_3 and O_2 gases to allow for unambiguous quantification.

Powder X-ray diffraction measurements (Fig. S5) were carried out on a Bruker D8 Discover with GADDS (General Area Detector Diffraction System), equipped with automated Laser-Video alignment system, rotating Cu anode (λ = 1.542 Å) and Hi-Star 2D detector. The instrument was operated in parallel-beam geometry with a 0.5 mm beam diameter and instrument-related peak broadening of 0.3° in 2 θ. All samples were scanned at 40 kV and 120 mA with a step size of 0.02°. Reference patterns were retrieved from ICSD and ICDD database (Mo: 42-1120, $CuInSe_2$: 40-1487).

References of ESI

1. K. M. O'Malley, C. Z. Li, H. L. Yip and A. K. Y. Jen, *Adv. Energy Mater.*, 2011, **2**, 82-86.
2. P. W. Liang, C. C. Chueh, S. T. Williams and A. K. Y. Jen, *Adv. Energy Mater.*, 2015, **5**, DOI: 10.1002/aenm.201402321.
3. C.-C. Chueh, C.-Z. Li and A. K.-Y. Jen, *Energy Environ. Sci.*, 2015, **8**, 1160-1189.
4. G. E. Eperon, S. D. Stranks, C. Menelaou, M. B. Johnston, L. M. Herz and H. J. Snaith, *Energy Environ. Sci.*, 2014, **7**, 982-988.
5. C.-Z. Li, C.-C. Chueh, H.-L. Yip, K. M. O'Malley, W.-C. Chen and A. K.-Y. Jen, *J. Mater. Chem.*, 2012, **22**, 8574-8578.
6. J. H. Kim, P.-W. Liang, S. T. Williams, C. Cho Namchul, Chu-Chen, M. S. Glaz, D. S. Ginger and A. K.-J. Jen, *Advanced Materials*, 2015, **27**, 695-701.
7. A. R. Uhl, J. K. Katahara and H. W. Hillhouse, *Energy & Environmental Science*, 2016, **9**, 130-134.